

Identification and molecular characterization of mutations in Nucleocapsid Phosphoprotein of SARS-CoV-2

Gajendra Kumar Azad ^{Corresp. 1}

¹ Department of Zoology, Patna University, Patna, Bihar, India

Corresponding Author: Gajendra Kumar Azad
Email address: gkazad@patnauniversity.ac.in

SARS-CoV-2 genome encodes four structural protein that include, Spike glycoprotein, Membrane protein, Envelope protein and Nucleocapsid Phosphoprotein (N-protein). The N-protein interacts with viral genomic RNA and helps in packaging. As the SARS-CoV-2 spread to almost all countries worldwide within 2-3 months; it also acquired mutations in its RNA genome. Therefore, this study was conducted with an aim to identify the variations present in N-protein of SARS-CoV-2. Here, we analysed 4163 reported sequence of N-protein from United States of America (USA) and compared with first reported sequence from Wuhan, China. Our study identified 107 mutations that reside all over the N-protein. Further, we show the high rate of mutations in intrinsically disordered regions (IDRs) of N-protein. Our study show 45% residues of IDR2 harbour mutations. The RNA binding domain (RBD) and dimerization domain of N-protein also have mutations at key residues. We further measured the effect of these mutations on N-protein stability and dynamicity and our data reveals that multiple mutations can cause considerable alterations. Altogether, our data strongly suggests that N-protein is one of the mutational hotspot proteins of SARS-CoV-2 that is changing rapidly and these mutations can potentially interferes with various aspects of N-protein functions including its interaction with RNA, oligomerization and signalling events.

1 TITLE

2 Identification and molecular characterization of mutations in Nucleocapsid Phosphoprotein of
3 SARS-CoV-2

4

5 AUTHORS

6 Gajendra Kumar Azad^{1#}

7

8 ¹Assistant Professor, Department of Zoology, Patna University, Patna-800005, Bihar (India)

9 #Corresponding Author:

10 Gajendra Kumar Azad

11 Email address: gkazard@patnauniversity.ac.in

12

13 Keywords: COVID-19; SARS-CoV-2; Mutations; Nucleocapsid Phosphoprotein (N-protein);

14 Infectious diseases; USA

15

16

17

18

19

20

21

22

23

24

25

26

27

28

29

30

31

32

33

34

35

36

37

38 ABSTRACT

39 SARS-CoV-2 genome encodes four structural protein that include, Spike glycoprotein,
40 Membrane protein, Envelope protein and Nucleocapsid Phosphoprotein (N-protein). The N-
41 protein interacts with viral genomic RNA and helps in packaging. As the SARS-CoV-2 spread to
42 almost all countries worldwide within 2-3 months; it also acquired mutations in its RNA genome.
43 Therefore, this study was conducted with an aim to identify the variations present in N-protein of
44 SARS-CoV-2. Here, we analysed 4163 reported sequence of N-protein from United States of
45 America (USA) and compared with first reported sequence from Wuhan, China. Our study
46 identified 107 mutations that reside all over the N-protein. Further, we show the high rate of
47 mutations in intrinsically disordered regions (IDRs) of N-protein. Our study show 45% residues
48 of IDR2 harbour mutations. The RNA binding domain (RBD) and dimerization domain of N-
49 protein also have mutations at key residues. We further measured the effect of these mutations
50 on N-protein stability and dynamicity and our data reveals that multiple mutations can cause
51 considerable alterations. Altogether, our data strongly suggests that N-protein is one of the
52 mutational hotspot proteins of SARS-CoV-2 that is changing rapidly and these mutations can
53 potentially interferes with various aspects of N-protein functions including its interaction with
54 RNA, oligomerization and signalling events.

55

56 INTRODUCTION

57 In the late December, 2019, Wuhan, the Hubei province of China, reported a surge in
58 hospitalisation due to pneumonia like symptoms (Zhu et al., 2020). The causative agent was
59 identified as a severe acute respiratory syndrome coronavirus 2 (SARS-CoV-2) that shares
60 close similarity with earlier known SARS-CoV (Chen et al., 2020). The SARS-CoV-2 is highly
61 contagious that lead to its rapid spread worldwide, and in March 2020, the World Health
62 Organization (WHO) declared the outbreak a pandemic. The disease caused by SARS-CoV-2
63 has been named as coronavirus disease 19 (COVID-19) that exhibits mild to severe respiratory
64 distress in the infected individuals. As of 28th June, 2020 the COVID-19 has affected all
65 countries worldwide with close to 10 million reported cases and 0.5 million confirmed deaths.
66 Further, the epidemiological studies revealed that the mortality rate from COVID-19 is
67 significantly higher among individuals over 60 years of age with weak immunity (Liu et al.,
68 2020).

69 The SARS-CoV-2 has positive sense, single stranded RNA genome of approximately 29.8 kb
70 (Wu et al., 2020b). The majority of viral genome encodes non-structural proteins that are
71 proteolytically processed from a single Orf1ab polypeptide. SARS-CoV-2 genome also encode
72 four structural proteins, including the Spike glycoprotein (S), Membrane protein (M), Envelope
73 protein (E) and Nucleocapsid Phosphoprotein (N) (Wu et al., 2020a). The S, M and E proteins
74 are located in the lipid bilayer of the virus and contribute to the formation of viral envelope;
75 however, the N-protein contributes to the viral genomic RNA packaging and remains embedded
76 in the central core of the virion. N-protein binds with viral genomic RNA and forms helical
77 structure to maintain the structural integrity of RNA genome (Chang et al., 2014). This is one of
78 the most abundant structural proteins encoded by the SARS-CoV-2 genome. The SARS-CoV-2
79 N-protein resembles N-protein from other RNA viruses, known to modulate host intracellular
80 machinery and also involved in the regulation of virus life cycle (McBride, van Zyl & Fielding,
81 2014). Evidence show that N-protein is recruited to the Replication-Transcription Complexes
82 (RTC) via Nsp3 and plays a crucial role in coronaviral life cycle (Cong et al., 2019). The
83 abrogation of this interaction impairs the stimulation of genomic RNA and viral mRNA
84 transcription in vivo and in vitro. Furthermore, the N-protein interactions with M promotes
85 completion of viral assembly by stabilizing N protein-RNA complex, inside the internal virion
86 (Astuti & Ysrafil, 2020).

87 The crystal structure of N-protein revealed two distinct domains at N and C terminus (Kang et
88 al., 2020). The domain present towards the N terminus is also known and RNA binding domain
89 (RBD). The C terminal side harbours dimerization domain which interacts with other N-protein to
90 make dimer. Apart from these two domains there are three intrinsically disordered regions
91 (IDRs) at N and C terminal ends as well as between the RBD and dimerization domain of N-
92 protein. Since, this protein plays critical role in packaging of SARS-CoV-2 RNA genome, the
93 mutations in N-protein or interfering its function can lead to diverse outcome on viral life cycle
94 (Rabi Ann Musah, 2005; Chenavas et al., 2013).

95 Moreover, the study of N-protein is also important because of its unique immunological
96 properties. For instance, earlier study with SARS N-protein has shown that this protein is a
97 potential candidate for vaccine development because it can induce a strong immunological
98 response (Liu et al., 2006). A recent study revealed that the B and T cell epitopes of N protein of
99 SARS-CoV-2 shows close resemblance with that of SARS-CoV indicating that immune targeting
100 of these identical epitopes may offer protection against this virus (Ahmed, Quadeer & McKay,
101 2020). Moreover, the sera of COVID-19 patients contains abundant amount of IgA, IgM and IgG
102 antibodies against N-protein antigen demonstrating the importance of this antigen in host

103 immunity and diagnostics (Shang et al., 2005; Zeng et al., 2020). Therefore, the N-protein is one
104 of the candidate target molecule that needs to be properly studied to understand its role in virus
105 pathogenesis, vaccine development and pharmacological implications. Here, we compared the
106 N-protein sequences obtained from USA with first reported sequence from China to identify the
107 variations present between them. We have identified 107 mutations and their impact on N-
108 protein structure and function are discussed.

109

110 MATERIALS AND METHODS

111 *Sequence retrieval from NCBI-virus-database*

112 The NCBI-virus-database stores the deposited sequences of SARS-CoV-2 which is updated
113 regularly as the new sequences are reported. As of 23rd June 2020, 4163 SARS-CoV-2
114 sequences of N-protein were deposited from USA. We downloaded these sequences and used
115 them for analysis in this study. The first reported N-protein sequence from Wuhan was used as
116 reference sequence or wild type sequence (Wu et al., 2020b). The protein accession
117 identification number of reference sequence used in this study is YP_009724397 and rest of the
118 4163 IDs (reported from USA) are mentioned in supplementary table 1.

119

120 *Multiple sequence alignment by Clustal-Omega program*

121 To identify the mutations present in the SARS-CoV-2 N-protein reported from USA, we did
122 multiple sequence alignments and compared them with the first reported N-protein sequence
123 (YP_009724397) from Wuhan, China. The multiple sequence alignment was performed using
124 Clustal Omega tool (Madeira et al., 2019).

125

126 *Calculation of free energy and vibrational entropy between wild type and mutant N-proteins*

127 In order to measure the impact of mutations identified in this study on the structural dynamicity
128 and stability of N-protein, we calculated the differences in free energy ($\Delta\Delta G$) and vibrational
129 entropy ($\Delta\Delta S_{vib}$) ENCoM between wild type and mutants. This analysis was performed by
130 DynaMut program (Rodrigues, Pires & Ascher, 2018). To perform DynaMut protein modelling
131 we used RCSB protein ID: 6VYO (Kang et al., 2020) for RBD molecular modelling and RCSB
132 protein ID: 6WJI for dimerization domain molecular modelling of N-protein. DynaMut also
133 provide the visual representation of fluctuation in protein structure. The blue colour represents
134 gain in rigidity and red colour represents gain in flexibility upon mutation.

135

136 RESULTS

137 *Identification of mutations in IDR1, IDR2 and IDR3 of N-protein*

138 The crystal structure of N-protein of SARS-CoV-2 has been recently solved (Kang et al., 2020),
139 the structural details show it is comprised of three distinct regions; the N terminal domain
140 (contains RNA binding domain), C terminal domain (contains dimerization domain) and IDRs as
141 shown in figure 1. There are three IDRs in N-protein; IDR1 (at the N terminal end), IDR2
142 (between RBD and CTD) and IDR3 (at the C terminal end). IDR2 is also referred as linker
143 region (LKR) because it connects RBD and dimerization domain of N-protein. In order to identify
144 the variations present in N-protein of SARS-CoV-2 reported from the USA, we performed
145 multiple sequence alignments. Here, we used Clustal Omega program to align 4163 N-protein
146 polypeptide sequences from USA and compared them with the first reported sequence from
147 Wuhan, China.

148 Our analysis identified eighteen mutations in IDR1 (Table1). The IDR1 is present from 1-43
149 residues towards the N terminal end of N-protein. These eighteen mutations correspond to
150 approximately 40% (18 out of 43) of the residues of IDR1. Among these the most frequently
151 mutated residues are Gly and Arg (both are mutated at four positions) and Pro residue is
152 mutated at three different positions in IDR1 (Table 1).

153 Similar analysis with IDR2 identified thirty six mutations which correspond to approximately 45%
154 of residues of IDR2 (Table 2). The IDR2 is present from 181-256 residues of the N-protein and
155 connects RBD and dimerization domains. The most frequently mutated residue in IDR2 was
156 found to be Ser, it is mutated at twelve positions. Further, the Ala, Gly and Arg residues are
157 mutated at five positions, respectively.

158 Similarly, we identified fifteen mutations in IDR3 (Table 3). The IDR3 is present from 365-419
159 residues towards the C terminal end of N-protein. Most notable mutations are Thr and Ala
160 residues are mutated at three positions and Pro, Asp, and Gln are mutated at two positions,
161 respectively (Table 3). Altogether, we identified sixty nine mutations in intrinsically disordered
162 regions IDR1, IDR2 and IDR3 of N-protein.

163

164 *Identification of mutations in RBD and dimerization domain of N-protein*

165 The RBD of N-protein starts from 44th residue till 180th residue. We mapped the mutation in this
166 region of N-protein and our analysis revealed presence of twenty two mutations (Table 4).

167 These twenty two mutations also correspond to approximately 16% of the residues of RBD. Our
168 mutational analysis shows the most frequently mutated residues are Pro and Ala at five
169 positions and Asp at three positions as shown in table 4.

170 Similar analysis with the dimerization domain of N-protein revealed that it harbours sixteen
171 mutations (Table 5). The dimerization domain of N-protein starts from 257th residue till 364th
172 residue. Our mutational analysis shows Thr is mutated at four positions and Asp at three
173 positions. Further, only 14 % residues are mutated in this domain which is least among all other
174 regions of the N-protein identified here. Altogether, we identified thirty eight mutations in RBD
175 and dimerization domain of N-protein. We have highlighted the location of amino acids in the
176 representative crystal structure of N-protein that are mutated in RBD (Figure 1B) and
177 dimerization domain (Figure 1C)

178 Subsequently, we also calculated the frequency of each mutation identified in this study. The
179 table 6 shows the top ten mutants arranged in descending order of their respective frequencies.
180 The R203K mutation is having the highest frequency of 4.9% followed by G204R with 4.7%.
181 Altogether, we have identified 107 mutations in N-protein that resides in its IDRs and RBD and
182 dimerization domain.

183

184 *Mutations causes alteration in dynamic stability of N-protein*

185 In order to understand the effect of mutations on the stability of the protein we calculated the
186 differences in free energy ($\Delta\Delta G$) between wild type and mutants. We performed this analysis
187 using DynaMut program. The positive $\Delta\Delta G$ corresponds to increase in stability while negative
188 $\Delta\Delta G$ corresponds to decrease in stability. We performed this analysis with all of the mutations
189 that reside in RBD and dimerization domain of N-protein. The IDRs do not have proper 3D
190 structure therefore; this analysis is not accurate for those regions. Our data revealed the
191 noticeable increase or decrease in free energy in various mutations as shown in table 6. The top
192 five positive and negative $\Delta\Delta G$ values are highlighted in table 6. The maximum increase in $\Delta\Delta G$
193 was observed for T271I (1.184 kcal/mol) and the highest negative $\Delta\Delta G$ was obtained for I292T
194 (-1.952 kcal/mol), both of these mutations reside in dimerization domain of N-protein.

195 We also measured the change in vibrational entropy energy ($\Delta\Delta S_{\text{vib}}\text{ENCoM}$) between the wild
196 type and the mutants present in RBD and dimerization domain of N-protein (Table 7).Vibration
197 entropy contributes to the configurational-entropy of the proteins (Goethe, Fita & Rubi, 2015).
198 The negative $\Delta\Delta S_{\text{vib}}\text{ENCoM}$ of mutant N-protein corresponds to the increase in rigidification and
199 positive $\Delta\Delta S_{\text{vib}}\text{ENCoM}$ corresponds to gain in flexibility of the protein structure. The maximum
200 positive $\Delta\Delta S_{\text{vib}}\text{ENCoM}$ was obtained for P364L (0.256 kcal.mol⁻¹.K⁻¹) and negative
201 $\Delta\Delta S_{\text{vib}}\text{ENCoM}$ was obtained for G284E (-0.844 kcal.mol⁻¹.K⁻¹). The variation in vibrational
202 entropy between wild type and mutant can also be visualised as shown in figure 2. The blue
203 colour corresponds to rigidification in protein structure and red colour corresponds to gain in

204 flexibility upon mutation. The top three positive and negative $\Delta\Delta S_{\text{vib}}\text{ENCoM}$ are shown in figure
205 2 (A-F). Altogether, the data obtained from $\Delta\Delta G$ and $\Delta\Delta S_{\text{vib}}\text{ENCoM}$ strongly suggests that the
206 mutations identified in this study can influence N-protein stability and dynamicity.

207

208 *Intramolecular interactions are altered due to mutations in N-protein*

209 Next, we sought to closely analyse the changes in the intramolecular interactions in some of the
210 mutants that exhibited significant alterations in $\Delta\Delta G$. We compared the intramolecular
211 interaction for T271I ($\Delta\Delta G$: 1.184 kcal/mol) and I292T ($\Delta\Delta G$: -1.952 kcal/mol) as these two
212 mutants showed maximum variations among thirty eight mutants present in RBD and
213 dimerization domain of N-protein (Table 4 and 5). Our data clearly showed the variations in the
214 interactions mediated by wild type and mutant residues in the pocket, where these amino acids
215 resides as shown in figure 3A-B (T271I) , and 3C-D (I292T). Altogether, our data strongly
216 suggests that the mutants identified in our study are affecting the dynamic stability as well as
217 intramolecular interactions in the N-protein.

218

219 DISCUSSIONS

220 SARS-CoV-2 is an RNA virus, a causative agent of COVID-19. This virus spread worldwide
221 within a span of few months and during its spread it also acquired mutations. Several recent
222 studies reported the appearance of mutations in SARS-CoV-2 proteins (Korber et al., 2020;
223 Pachetti et al., 2020; Chand, Banerjee & Azad, 2020). This study was performed with an aim to
224 identify mutations in N-protein which is one of the main structural proteins of SARS-CoV-2.
225 Here, we analysed 4163 sequences of N-protein from USA and identified 107 mutations upon
226 comparison from first reported sequences of the same protein from Wuhan, China. We also
227 observed around 64% (69 out of 107) of these mutations reside in the IDRs of N-protein. Among
228 IDRs, the IDR2 harbours 36 mutations that correspond to the most number of mutations
229 observed in a single distinct region of the N-protein.

230 Earlier studies demonstrated that Ser and Arg-rich linker region (IDR2) plays indispensable role
231 in intracellular signalling events primarily by phosphorylation at Ser residues (Wootton, Rowland
232 & Yoo, 2002; McBride, van Zyl & Fielding, 2014). The wild type LKR/ IDR2 contains sixteen Ser
233 residues, and our study revealed that out of those, twelve serine residues are mutated (table 2).
234 Therefore, we can safely assume that these mutations of Ser residues might contribute to
235 alteration of phosphorylation dependent signalling. A recent study shows that S197, S202,
236 R203 and G204 are important sites of phosphorylation by Aurora kinase A/B, GSK-3 as well as
237 for its interactions with 14-3-3 protein (Tung & Limtung, 2020). Surprisingly, our study report

238 mutation in all of these four residues suggesting that these mutant might have altered
239 phosphorylation signaling. We have also observed that R203 and G204 is the most frequently
240 mutated residue of N-protein (Table 6). Similar observations were also reported from other
241 locations (Franco-Munoz et al., 2020). Furthermore, two recent independent studies revealed
242 that SARS-CoV-2 is capable of suppressing the type-I IFN innate immune pathway possibly due
243 to the role of N-protein in signalling events (Blanco-Melo et al., 2020; Zhou et al., 2020a) which
244 can potentially alter the virulence of SARS-CoV-2.

245 We also measured $\Delta\Delta G$ and $\Delta\Delta S_{\text{vib}}\text{ENCoM}$ for the mutants that reside in the RBD and
246 dimerization domain of N-protein. The four mutants that exhibited highest values for $\Delta\Delta G$ and
247 $\Delta\Delta S_{\text{vib}}\text{ENCoM}$ identified in our study are T271I, I292T, G284E and P364L. Since, all of them
248 are in the dimerization domain; therefore, it is possible that these mutations might lead to
249 alteration in the dimerization potential of N-protein. The structural study of N-protein (C terminal
250 domain) has revealed that residue 247-279 are essential for RNA binding (Zhou et al., 2020b)
251 which harbours seven mutations (T247A, K249R, S250F, A252S, S255A, V270L
252 T271I). The occurrence of these mutations in C terminal domain could possibly affect its
253 interaction with RNA that might translate into viral RNA packaging and stability. Furthermore,
254 the N-protein is also proposed as a candidate for vaccine development because it is known to
255 elicit strong immunological response in SARS-CoV infected patients (Lin et al., 2003). A recent
256 study shows that several B cell epitope of SARS-CoV were identical with SARS-CoV-2 (Ahmed,
257 Quadeer & McKay, 2020). This study revealed that one of the most important B and T cell
258 epitope lies between residues 305-340 of N-protein; however, our study identified multiple
259 mutations including, P309L, M322I, S327L, T329M, T334I, D340G, D340N in that stretch.
260 Therefore, it is possible that due to these mutations the properties of epitope might change that
261 can affect host immunological response. Another mutation, P344S mutation has been
262 implicated to decrease the protein stability (Khan et al., 2020). Hence, the development of
263 vaccines that target SARS-COV-2 N-protein must consider the mutations that occur in various
264 populations and locations.

265 Evidences indicate that the N-protein of coronaviruses functions as an RNA chaperones (Zúñiga
266 et al., 2007, 2010) and also contributes to packaging and maintenance of the RNA genome. It is
267 also involved in RNA metabolism because N-protein interaction assays have shown the core
268 stress granule components G3BP1 and G3BP2 are its interacting partners (Gordon et al.,
269 2020). This interaction can either enhance stress granule induction or inhibit stress granule
270 formation by sequestering G3BP1/G3BP2 (Hou et al., 2017). Hence, the drugs that can either
271 inhibit the interactions of RNA with N-protein or interfere with dimerization of N-protein can be a

272 potential antiviral candidates (Lo et al., 2013). One such drug is Nucleozin and its derivatives
273 that targets ribonucleoprotein formation in influenza virus by interfering N-protein
274 oligomerization (Gerritz et al., 2011). Furthermore, a recent study was conducted to identify
275 inhibitors of SARS-CoV-2 N-protein, identified various promising candidate drugs including
276 Conivaptan, Ergotamine, Venetoclax and Rifapentine (Onat Kadioglu, 2020). These candidate
277 drugs interact with the residues that are either mutated (residue 154, 155, 156, 166) or are in
278 the close vicinity of the mutations (residue 67, 81, 163, 169) identified in our study. Furthermore,
279 bioinformatics analysis predicted Dihydroergotamine, Rifabutin and Nystatin as a potential
280 candidate drugs (Onat Kadioglu, 2020) that interacts with a stretch of residues (from residues
281 150 to 160) of N-protein. Surprisingly, our study revealed that this stretch harbour four mutations
282 (151, 152, 154 and 156), which can potentially alter the interactions of these drugs with N-
283 protein. Altogether, the mutation revealed in this study can interfere with various aspects of N-
284 protein functions that include oligomerization, interaction with RNA and interference in N-protein
285 mediated signalling events.

286

287

288 CONCLUSIONS

289 In this study we identified 107 mutations in N-protein of SARS-CoV-2 reported from USA.
290 Further, we demonstrate these mutations can potentially alter dynamic stability of N-protein.
291 Altogether, the data presented here, warrants further investigations to understand its impact on
292 SARS-CoV-2 phenotype and drugs that target N-protein.

293

294 ACKNOWLEDGEMENTS

295 We would like to acknowledge the Department of Zoology, Patna University, Patna, Bihar (India)
296 for providing infrastructural support for this study.

297

298 FIGURE AND TABLE LEGENDS

299 Figure 1: The schematic structure of Nucleocapsid Phosphoprotein (N-protein) of SARS-CoV-2.
300 The N-protein comprising of 419 residues is shown. The RNA binding domain, dimerization
301 domain, intrinsically disordered regions including IRD1, IRD2, and IRD3 are labelled. B-C)
302 Cartoon representation of crystal structure of the RNA binding domain and dimerization domain
303 of N-protein. The stick shows the location of residues that are mutated in the respective
304 domains. The structural representations are made using Autodock software.

305

306 Figure 2: Visual representation of Δ Vibrational Entropy Energy between Wild-Type and Mutant
307 N-protein. The amino acids residues are colored according to the vibrational entropy change as
308 a consequence of mutation of N-protein. **BLUE** represents a rigidification of the structure and
309 **RED** a gain in flexibility. (A-C) represents the top three mutants that show rigidification in
310 structure upon mutation. (D-F) represents the top three mutants that show gain in flexibility upon
311 mutation. Each panel also shows the mutation and the location of the residues.

312

313 Figure 3: Visual representation of interatomic interactions contributed by T271I and I292T of N-
314 protein. Both of these mutants showed maximum positive and negative $\Delta\Delta G$ among mutants
315 present in RBD and dimerization domain of N-protein. (A-B) represents threonine to isoleucine
316 substitution at 271st position; (C-D) represents isoleucine to threonine substitution at 292nd
317 position. Wild-type and mutant residues are represented in light-green color. The interactions
318 made by wild type and mutant residues are highlighted in each panel. The polar interactions are
319 depicted in red dotted line, hydrophobic interaction in green and weak hydrogen bonds in
320 orange.

321

322 Table 1: The table show the location and details of mutations identified in IDR1 of N-protein.

323

324 Table 2: The table show the location and details of mutations identified in IDR2.

325

326 Table 3: The table show the location and details of mutations identified in IDR3.

327

328 Table 4: The table show the location and details of mutations identified in RBD of N-protein.

329

330 Table 5: The table show the location and details of mutations identified in dimerization domain
331 of N-protein.

332

333 Table 6: The frequency of top ten mutations observed in our study

334

335 Table 7: The table show the $\Delta\Delta G$ and $\Delta\Delta S_{vib}$ ENCoM of the mutants present in RBD and
336 dimerization domain of N-protein. DynaMut program was used to calculate both parameters.

337 The top five positive and negative $\Delta\Delta G$ values are highlighted in bold digits. The top three

338 positive and negative $\Delta\Delta S_{vib}$ ENCoM values are highlighted in bold digits.

339

340 REFERENCES

- 341 Ahmed SF, Quadeer AA, McKay MR. 2020. Preliminary identification of potential vaccine
342 targets for the COVID-19 Coronavirus (SARS-CoV-2) Based on SARS-CoV Immunological
343 Studies. *Viruses*. DOI: 10.3390/v12030254.
- 344 Astuti I, Ysrafil. 2020. Severe Acute Respiratory Syndrome Coronavirus 2 (SARS-CoV-2): An
345 overview of viral structure and host response. *Diabetes and Metabolic Syndrome: Clinical
346 Research and Reviews*. DOI: 10.1016/j.dsx.2020.04.020.
- 347 Blanco-Melo D, Nilsson-Payant BE, Liu WC, Uhl S, Hoagland D, Møller R, Jordan TX, Oishi K,
348 Panis M, Sachs D, Wang TT, Schwartz RE, Lim JK, Albrecht RA, tenOever BR. 2020.
349 Imbalanced Host Response to SARS-CoV-2 Drives Development of COVID-19. *Cell*. DOI:
350 10.1016/j.cell.2020.04.026.
- 351 Chand GB, Banerjee A, Azad GK. 2020. Identification of novel mutations in RNA-dependent
352 RNA polymerases of SARS-CoV-2 and their implications on its protein structure. *PeerJ*
353 8:e9492. DOI: 10.7717/peerj.9492.
- 354 Chang CK, Hou MH, Chang CF, Hsiao CD, Huang TH. 2014. The SARS coronavirus
355 nucleocapsid protein - Forms and functions. *Antiviral Research*. DOI:
356 10.1016/j.antiviral.2013.12.009.
- 357 Chen N, Zhou M, Dong X, Qu J, Gong F, Han Y, Qiu Y, Wang J, Liu Y, Wei Y, Xia J, Yu T,
358 Zhang X, Zhang L. 2020. Epidemiological and clinical characteristics of 99 cases of 2019
359 novel coronavirus pneumonia in Wuhan, China: a descriptive study. *The Lancet*. DOI:
360 10.1016/S0140-6736(20)30211-7.
- 361 Chenavas S, Cre´pin T, Delmas B, Ruigrok RWH, Slama-Schwok A. 2013. Influenza virus
362 nucleoprotein: Structure, RNA binding, oligomerization and antiviral drug target. *Future
363 Microbiology*. DOI: 10.2217/fmb.13.128.
- 364 Cong Y, Ulasli M, Schepers H, Mauthe M, V'kovski P, Kriegenburg F, Thiel V, de Haan CAM,
365 Reggiori F. 2019. Nucleocapsid Protein Recruitment to Replication-Transcription
366 Complexes Plays a Crucial Role in Coronaviral Life Cycle. *Journal of Virology*. DOI:
367 10.1128/jvi.01925-19.
- 368 Franco-Munoz C, Alvarez-Diaz DA, Laiton-Donato K, Wiesner M, Escandon P, Usme-Ciro JA,
369 Franco-Sierra ND, Florez-Sanchez AC, Gomez-Rangel S, Calderon LDR, Ramirez JB,
370 Baez EO, Walteros DM, Martinez MLO, Mercado-Reyes M. 2020. Substitutions in Spike
371 and Nucleocapsid proteins of SARS-CoV-2 circulating in Colombia. *medRxiv*. DOI:
372 10.1101/2020.06.02.20120782.
- 373 Gerritz SW, Cianci C, Kim S, Pearce BC, Deminie C, Discotto L, McAuliffe B, Minassian BF, Shi

- 374 S, Zhu S, Zhai W, Pendri A, Li G, Poss MA, Edavettal S, McDonnell PA, Lewis HA, Maskos
375 K, Morfl M, Kiefersauer R, Steinbacher S, Baldwin ET, Metzler W, Bryson J, Healy MD,
376 Philip T, Zoeckler M, Schartman R, Sinz M, Leyva-Grado VH, Hoffmann HH, Langley DR,
377 Meanwell NA, Krystal M. 2011. Inhibition of influenza virus replication via small molecules
378 that induce the formation of higher-order nucleoprotein oligomers. *Proceedings of the*
379 *National Academy of Sciences of the United States of America*. DOI:
380 10.1073/pnas.1107906108.
- 381 Gordon DE, Jang GM, Bouhaddou M, Xu J, Obernier K, White KM, O'Meara MJ, Rezelj V V.,
382 Guo JZ, Swaney DL, Tummino TA, Huettenhain R, Kaake RM, Richards AL, Tutuncuoglu
383 B, Foussard H, Batra J, Haas K, Modak M, Kim M, Haas P, Polacco BJ, Braberg H, Fabius
384 JM, Eckhardt M, Soucheray M, Bennett MJ, Cakir M, McGregor MJ, Li Q, Meyer B, Roesch
385 F, Vallet T, Mac Kain A, Miorin L, Moreno E, Naing ZZC, Zhou Y, Peng S, Shi Y, Zhang Z,
386 Shen W, Kirby IT, Melnyk JE, Chorba JS, Lou K, Dai SA, Barrio-Hernandez I, Memon D,
387 Hernandez-Armenta C, Lyu J, Mathy CJP, Perica T, Pilla KB, Ganesan SJ, Saltzberg DJ,
388 Rakesh R, Liu X, Rosenthal SB, Calviello L, Venkataramanan S, Liboy-Lugo J, Lin Y,
389 Huang XP, Liu YF, Wankowicz SA, Bohn M, Safari M, Ugur FS, Koh C, Savar NS, Tran
390 QD, Shengjuler D, Fletcher SJ, O'Neal MC, Cai Y, Chang JCJ, Broadhurst DJ, Klippsten S,
391 Sharp PP, Wenzell NA, Kuzuoglu D, Wang HY, Trenker R, Young JM, Cavero DA, Hiatt J,
392 Roth TL, Rathore U, Subramanian A, Noack J, Hubert M, Stroud RM, Frankel AD,
393 Rosenberg OS, Verba KA, Agard DA, Ott M, Emerman M, Jura N, von Zastrow M, Verdin
394 E, Ashworth A, Schwartz O, d'Enfert C, Mukherjee S, Jacobson M, Malik HS, Fujimori DG,
395 Ideker T, Craik CS, Floor SN, Fraser JS, Gross JD, Sali A, Roth BL, Ruggero D, Taunton J,
396 Kortemme T, Beltrao P, Vignuzzi M, García-Sastre A, Shokat KM, Shoichet BK, Krogan
397 NJ. 2020. A SARS-CoV-2 protein interaction map reveals targets for drug repurposing.
398 *Nature*. DOI: 10.1038/s41586-020-2286-9.
- 399 Hou S, Kumar A, Xu Z, Airo AM, Stryapunina I, Wong CP, Branton W, Tchesnokov E, Götte M,
400 Power C, Hobman TC. 2017. Zika Virus Hijacks Stress Granule Proteins and Modulates
401 the Host Stress Response. *Journal of Virology*. DOI: 10.1128/jvi.00474-17.
- 402 Kang S, Yang M, Hong Z, Zhang L, Huang Z, Chen X, He S, Zhou Z, Zhou Z, Chen Q, Yan Y,
403 Zhang C, Shan H, Chen S. 2020. Crystal structure of SARS-CoV-2 nucleocapsid protein
404 RNA binding domain reveals potential unique drug targeting sites. *Acta Pharmaceutica*
405 *Sinica B*. DOI: 10.1016/j.apsb.2020.04.009.
- 406 Khan MI, Khan ZA, Baig MH, Ahmad I, Farouk A-E, Song YG, Dong J-J. 2020. Comparative
407 genome analysis of novel coronavirus (SARS-CoV-2) from different geographical locations

- 408 and the effect of mutations on major target proteins: An in silico insight. *PloS one*
409 15:e0238344. DOI: 10.1371/journal.pone.0238344.
- 410 Korber B, Fischer W, Gnanakaran SG, Yoon H, Theiler J, Abfalterer W, Foley B, Giorgi EE,
411 Bhattacharya T, Parker MD, Partridge DG, Evans CM, Silva T de, LaBranche CC,
412 Montefiori DC, Group SC-19 G. 2020. Spike mutation pipeline reveals the emergence of a
413 more transmissible form of SARS-CoV-2. *bioRxiv*. DOI: 10.1101/2020.04.29.069054.
- 414 Lin Y, Shen X, Yang RF, Li YX, Ji YY, He YY, Shi MD, Lu W, Shi TL, Wang J, Wang HX, Jiang
415 HL, Shen JH, Xie YH, Wang Y, Pei G, Shen BF, Wu JR, Sun B. 2003. Identification of an
416 epitope of SARS-coronavirus nucleocapsid protein. *Cell research*. DOI:
417 10.1038/sj.cr.7290158.
- 418 Liu K, Chen Y, Lin R, Han K. 2020. Clinical features of COVID-19 in elderly patients: A
419 comparison with young and middle-aged patients. *Journal of Infection*. DOI:
420 10.1016/j.jinf.2020.03.005.
- 421 Liu SJ, Leng CH, Lien SP, Chi HY, Huang CY, Lin CL, Lian WC, Chen CJ, Hsieh SL, Chong P.
422 2006. Immunological characterizations of the nucleocapsid protein based SARS vaccine
423 candidates. *Vaccine*. DOI: 10.1016/j.vaccine.2006.01.058.
- 424 Lo YS, Lin SY, Wang SM, Wang CT, Chiu YL, Huang TH, Hou MH. 2013. Oligomerization of the
425 carboxyl terminal domain of the human coronavirus 229E nucleocapsid protein. *FEBS*
426 *Letters*. DOI: 10.1016/j.febslet.2012.11.016.
- 427 Madeira F, Park YM, Lee J, Buso N, Gur T, Madhusoodanan N, Basutkar P, Tivey ARN, Potter
428 SC, Finn RD, Lopez R. 2019. The EMBL-EBI search and sequence analysis tools APIs in
429 2019. *Nucleic acids research*. DOI: 10.1093/nar/gkz268.
- 430 McBride R, van Zyl M, Fielding BC. 2014. The coronavirus nucleocapsid is a multifunctional
431 protein. *Viruses*. DOI: 10.3390/v6082991.
- 432 Onat Kadioglu MSHJGTE. 2020. Identification of novel compounds against three targets of
433 SARS CoV2 coronavirus by combined virtual screening and supervised machine learning .
434 *Bull World Health Organ*. DOI: 10.2471/BLT.20.251561.
- 435 Pachetti M, Marini B, Benedetti F, Giudici F, Mauro E, Storici P, Masciovecchio C, Angeletti S,
436 Ciccozzi M, Gallo RC, Zella D, Ippodrino R. 2020. Emerging SARS-CoV-2 mutation hot
437 spots include a novel RNA-dependent-RNA polymerase variant. *Journal of Translational*
438 *Medicine*. DOI: 10.1186/s12967-020-02344-6.
- 439 Rabi Ann Musah. 2005. The HIV-1 Nucleocapsid Zinc Finger Protein as a Target of
440 Antiretroviral Therapy. *Current Topics in Medicinal Chemistry*. DOI:
441 10.2174/1568026043387331.

- 442 Rodrigues CHM, Pires DEV, Ascher DB. 2018. DynaMut: Predicting the impact of mutations on
443 protein conformation, flexibility and stability. *Nucleic Acids Research*. DOI:
444 10.1093/nar/gky300.
- 445 Shang B, Wang XY, Yuan JW, Vabret A, Wu XD, Yang RF, Tian L, Ji YY, Deubel V, Sun B.
446 2005. Characterization and application of monoclonal antibodies against N protein of
447 SARS-coronavirus. *Biochemical and Biophysical Research Communications*. DOI:
448 10.1016/j.bbrc.2005.08.032.
- 449 Tung HYL, Limtung P. 2020. Mutations in the phosphorylation sites of SARS-CoV-2 encoded
450 nucleocapsid protein and structure model of sequestration by protein 14-3-3. *Biochemical
451 and Biophysical Research Communications*. DOI: 10.1016/j.bbrc.2020.08.024.
- 452 Wootton SK, Rowland RRR, Yoo D. 2002. Phosphorylation of the Porcine Reproductive and
453 Respiratory Syndrome Virus Nucleocapsid Protein. *Journal of Virology*. DOI:
454 10.1128/jvi.76.20.10569-10576.2002.
- 455 Wu A, Peng Y, Huang B, Ding X, Wang X, Niu P, Meng J, Zhu Z, Zhang Z, Wang J, Sheng J,
456 Quan L, Xia Z, Tan W, Cheng G, Jiang T. 2020a. Genome Composition and Divergence of
457 the Novel Coronavirus (2019-nCoV) Originating in China. *Cell Host and Microbe*. DOI:
458 10.1016/j.chom.2020.02.001.
- 459 Wu F, Zhao S, Yu B, Chen YM, Wang W, Song ZG, Hu Y, Tao ZW, Tian JH, Pei YY, Yuan ML,
460 Zhang YL, Dai FH, Liu Y, Wang QM, Zheng JJ, Xu L, Holmes EC, Zhang YZ. 2020b. A
461 new coronavirus associated with human respiratory disease in China. *Nature*. DOI:
462 10.1038/s41586-020-2008-3.
- 463 Zeng W, Liu G, Ma H, Zhao D, Yang Y, Liu M, Mohammed A, Zhao C, Yang Y, Xie J, Ding C,
464 Ma X, Weng J, Gao Y, He H, Jin T. 2020. Biochemical characterization of SARS-CoV-2
465 nucleocapsid protein. *Biochemical and Biophysical Research Communications*. DOI:
466 10.1016/j.bbrc.2020.04.136.
- 467 Zhou Z, Ren L, Zhang L, Zhong J, Xiao Y, Jia Z, Guo L, Yang J, Wang C, Jiang S, Yang D,
468 Zhang G, Li H, Chen F, Xu Y, Chen M, Gao Z, Yang J, Dong J, Liu B, Zhang X, Wang W,
469 He K, Jin Q, Li M, Wang J. 2020a. Heightened Innate Immune Responses in the
470 Respiratory Tract of COVID-19 Patients. *Cell Host and Microbe*. DOI:
471 10.1016/j.chom.2020.04.017.
- 472 Zhou R, Zeng R, von Brunn A, Lei J. 2020b. Structural characterization of the C-terminal
473 domain of SARS-CoV-2 nucleocapsid protein. *Molecular Biomedicine* 1:2. DOI:
474 10.1186/s43556-020-00001-4.
- 475 Zhu N, Zhang D, Wang W, Li X, Yang B, Song J, Zhao X, Huang B, Shi W, Lu R, Niu P, Zhan F,

476 Ma X, Wang D, Xu W, Wu G, Gao GF, Tan W. 2020. A novel coronavirus from patients
477 with pneumonia in China, 2019. *New England Journal of Medicine*. DOI:
478 10.1056/NEJMoa2001017.

479 Zúñiga S, Cruz JLG, Sola I, Mateos-Gómez PA, Palacio L, Enjuanes L. 2010. Coronavirus
480 Nucleocapsid Protein Facilitates Template Switching and Is Required for Efficient
481 Transcription. *Journal of Virology*. DOI: 10.1128/jvi.02011-09.

482 Zúñiga S, Sola I, Moreno JL, Sabella P, Plana-Durán J, Enjuanes L. 2007. Coronavirus
483 nucleocapsid protein is an RNA chaperone. *Virology*. DOI: 10.1016/j.virol.2006.07.046.
484

Table 1 (on next page)

IDR1 Mutations

The table show the location and details of mutations identified in IDR1 of N-protein.

1 Table 1:

S. No.	Wild type residue	Position of mutation	Mutated residue
1	Asp	3	Tyr
2	Asn	4	Asp
3	Pro	6	Thr
4	Gln	9	His
5	Pro	13	Leu
6	Arg	14	His
7	Gly	18	Cys
8	Gly	19	Arg
9	Pro	20	Leu
10	Asp	22	Tyr
11	Ser	23	Thr
12	Gly	30	Ala
13	Glu	31	Asp
14	Arg	32	Leu
15	Gly	34	Leu
16	Ala	35	Thr
17	Arg	36	Leu
18	Arg	40	Cys
19	Arg	40	Leu

2

Table 2 (on next page)

IDR2 mutations

The table show the location and details of mutations identified in IDR2.

1 Table 2:

S. No.	Wild type residue	Position of mutation	Mutated residue
1	Ser	183	Tyr
2	Arg	185	Cys
3	Arg	185	Leu
4	Ser	187	Leu
5	Ser	188	Leu
6	Ser	190	Ile
7	Arg	191	Leu
8	Asn	192	Ser
9	Ser	193	Ile
10	Ser	194	Leu
11	Arg	195	Ile
12	Ser	197	Leu
13	Pro	199	Ser
14	Ser	202	Asn
15	Arg	203	Lys
16	Arg	203	Met
17	Gly	204	Arg
18	Thr	205	Ile
19	Ala	208	Gly
20	Arg	209	Lys
21	Arg	209	Thr
22	Ala	211	Ser
23	Gly	212	Cys
24	Asn	213	Tyr
25	Gly	215	Ser
26	Ala	218	Val
27	Ala	220	Thr
28	Gln	229	His
29	Ser	232	Arg
30	Ser	232	Thr
31	Met	234	Ile
32	Ser	235	Pro
33	Ser	235	Phe
34	Gly	236	Val
35	Gly	238	Cys
36	Gly	243	Cys
37	Thr	247	Ala
38	Lys	249	Arg
39	Ser	250	Phe

40	Ala	252	Ser
41	Ser	255	Ala

2

Table 3 (on next page)

IDR3 mutations

The table show the location and details of mutations identified in IDR3.

1 Table 3:

S. No.	Wild type residue	Position of mutation	Mutated residue
1	Pro	365	Ser
2	Pro	365	Leu
3	Asp	377	Tyr
4	Asp	377	Gly
5	Thr	379	Ile
6	Gln	380	His
7	Ala	381	Val
8	Pro	383	Ser
9	Pro	383	Leu
10	Gln	386	Lys
11	Gln	386	His
12	Thr	391	Ile
13	Thr	393	Ile
14	Ala	397	Ser
15	Ala	398	Val
16	Asp	399	Glu
17	Ser	413	Ile
18	Ser	416	Leu

2

3

4

Table 4(on next page)

RBD mutations

The table show the location and details of mutations identified in RBD of N-protein

1 Table 4:

S. No.	Wild type residue	Position of mutation	Mutated residue
1	Pro	46	Ser
2	Glu	62	Val
3	Pro	67	Ser
4	Asp	81	Tyr
5	Ala	90	Ser
6	Ala	119	Ser
7	Pro	122	Leu
8	Ala	125	Thr
9	Asp	128	Tyr
10	Asn	140	Thr
11	Pro	142	Ser
12	Asp	144	Tyr
13	Asp	144	His
14	Ile	146	Phe
15	Pro	151	Leu
16	Ala	152	Ser
17	Asn	154	Tyr
18	Ala	156	Ser
19	Gln	163	Arg
20	Thr	166	Ile
21	Lys	169	Arg
22	Ser	180	Ile

2

Table 5 (on next page)

Dimerization domain mutations

The table show the location and details of mutations identified in dimerization domain of N-protein.

1 Table 5:

S. No.	Wild type residue	Position of mutation	Mutated residue
1	Val	270	Leu
2	Thr	271	Ile
3	Gly	284	Glu
4	Gln	289	His
5	Ile	292	Thr
6	Gln	294	Leu
7	Asp	297	Val
8	Pro	309	Leu
9	Met	322	Ile
10	Ser	327	Leu
11	Thr	329	Met
12	Thr	334	Ile
13	Asp	340	Gly
14	Asp	340	Asn
15	Asp	348	Tyr
16	Thr	362	Ile
17	Pro	364	Leu

2

Table 6 (on next page)

Frequency of N-protein mutations

The frequency of top 10 mutations observed in this study

1 Table 6:

Mutation	Number of samples that harbour the mutation	% frequency
R203K	207	4.97357
G204R	196	4.709274
E62V	39	0.937049
A208G	24	0.576646
S183Y	20	0.480538
S194L	18	0.432484
T362I	16	0.384431
T205I	15	0.360404
P13L	11	0.264296
R185C	10	0.240269

2

Table 7 (on next page) $\Delta\Delta G$ and $\Delta\Delta S_{vib}$ ENCoM calculations

The table show the $\Delta\Delta G$ and $\Delta\Delta S_{vib}$ ENCoM of the mutants present in RBD and dimerization domain of N-protein. DynaMut programme was used to calculate both parameters. The top five positive and negative $\Delta\Delta G$ values are highlighted in bold digits. The top three positive and negative $\Delta\Delta S_{vib}$ ENCoM values are highlighted in bold digits.

1 Table 7:

S. No.	Mutant	PDB ID	$\Delta\Delta G$ (kcal/mol)	$\Delta\Delta S_{vibENCoM}$ (kcal.mol ⁻¹ .K ⁻¹)
1	E62V	6VYO	0.105	0.091
2	P67S	6VYO	-0.486	0.16
3	D81Y	6VYO	0.454	-0.425
4	A90S	6VYO	0.274	0.043
5	A119S	6VYO	0.073	-0.069
6	P122L	6VYO	-0.166	-0.049
7	A125T	6VYO	-0.565	-0.022
8	D128Y	6VYO	0.846	-0.236
9	N140T	6VYO	0.318	-0.177
10	P142S	6VYO	0.26	-0.17
11	D144Y	6VYO	0.291	-0.293
12	D144H	6VYO	-0.036	0.06
13	I146F	6VYO	0.708	-0.837
14	P151L	6VYO	0.771	-0.14
15	A152S	6VYO	0.298	-0.051
16	N154Y	6VYO	-0.096	-0.063
17	A156S	6VYO	0.428	-0.256
18	Q163R	6VYO	-0.092	-0.017
19	T166I	6VYO	0.194	-0.055
20	K169R	6VYO	0.231	0.077
21	V270L	6WJI	0.679	-0.194
22	T271I	6WJI	1.184	-0.472
23	G284E	6WJI	0.553	-0.844
24	Q289H	6WJI	0.18	0.181
25	I292T	6WJI	-1.952	0.186
26	Q294L	6WJI	0.447	-0.078
27	D297V	6WJI	-0.113	-0.072
28	P309L	6WJI	0.887	-0.524
29	M322I	6WJI	-0.348	0.045
30	S327L	6WJI	0.894	-0.259
31	T329M	6WJI	0.569	-0.189
32	T334I	6WJI	0.236	-0.115
33	D340G	6WJI	0.398	-0.114
34	D340N	6WJI	0.194	-0.088
35	D348Y	6WJI	0.136	-0.121
36	T362I	6WJI	0.396	0.047
37	P364L	6WJI	-0.061	0.256

2

Figure 1

The schematic structure of Nucleocapsid Phosphoprotein (N protein) of SARS-CoV-2.

The schematic structure of Nucleocapsid Phosphoprotein (N-protein) of SARS-CoV-2. The N-protein comprising of 419 residues is shown. The RNA binding domain, dimerization domain, intrinsically disordered regions including IRD1, IRD2, and IRD3 are labelled. B-C) Cartoon representation of crystal structure of the RNA binding domain and dimerization domain of N-protein. The stick shows the location of residues that are mutated in the respective domains. The structural representations are made using Autodock software.

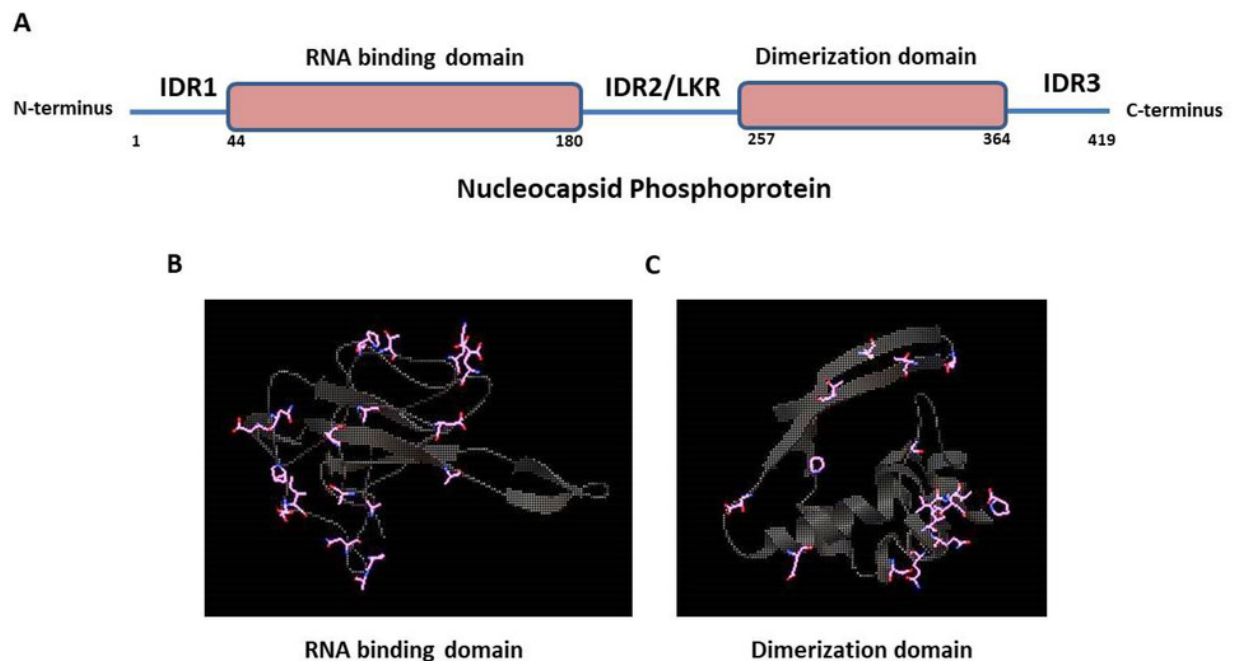


Figure 2

Visual representation of Δ Vibrational Entropy Energy between Wild-Type and Mutant N protein.

The amino acids residues are colored according to the vibrational entropy change as a consequence of mutation of N-protein. **BLUE** represents a rigidification of the structure and **RED** a gain in flexibility. (A-C) represents the top three mutants that show rigidification in structure upon mutation. (D-F) represents the top three mutants that show gain in flexibility upon mutation. Each panel also shows the mutation and the location of the residues.

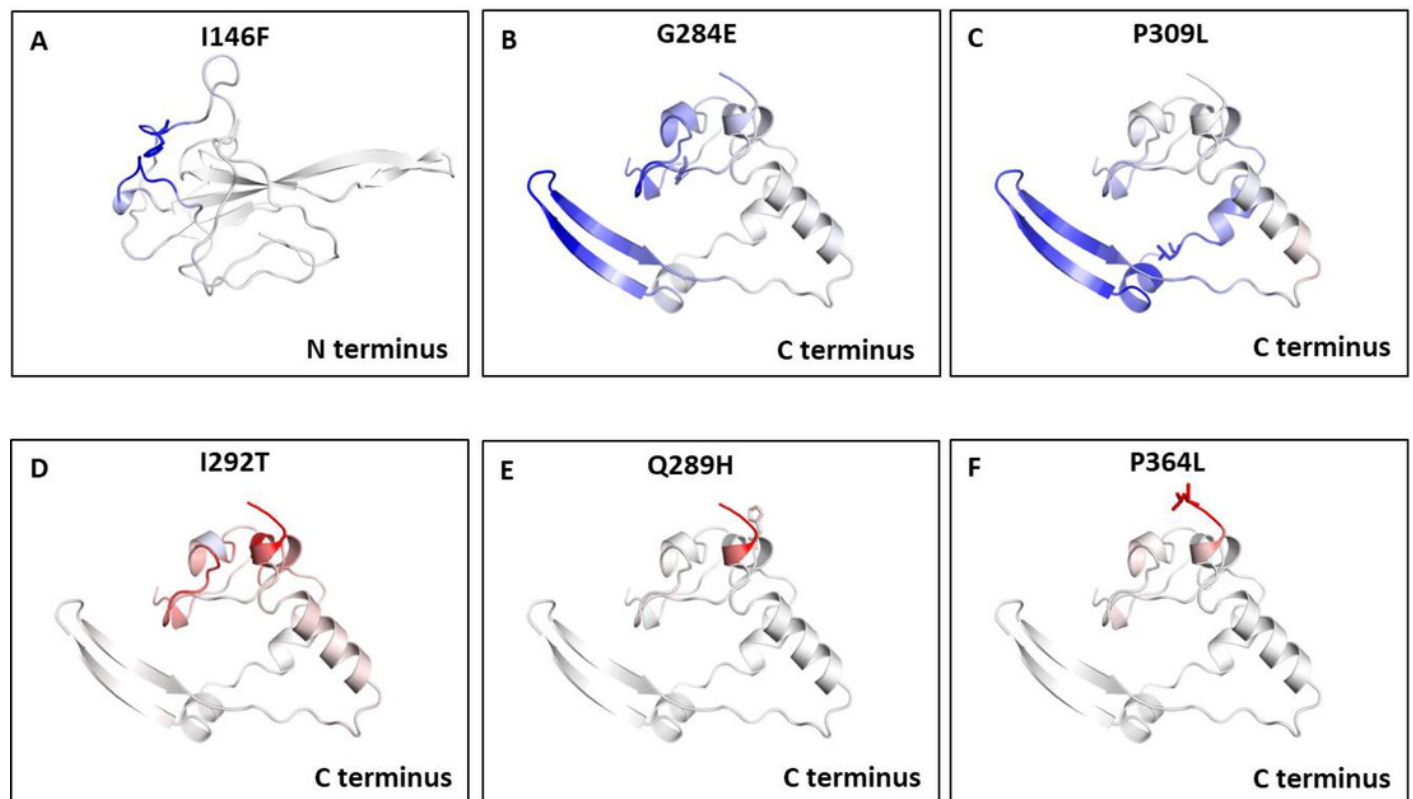


Figure 3

Analysis of interatomic interactions.

Visual representation of interatomic interactions contributed by T271I and I292T of N-protein. Both of these mutants showed maximum positive and negative $\Delta\Delta G$ among mutants present in RBD and dimerization domain of N-protein. (A-B) represents threonine to isoleucine substitution at 271st position; (C-D) represents isoleucine to threonine substitution at 292nd position. Wild-type and mutant residues are represented in light-green color. The interactions made by wild type and mutant residues are highlighted in each panel. The polar interactions are depicted in red dotted line, hydrophobic interaction in green and weak hydrogen bonds in orange.

